Springer

KSME

Journal of Mechanical Science and Technology 30 (3) (2016) 1021~1035
www.springerlink.com/content/1738-494x(Print)/1976-3824(Online)
DOI 10.1007/s12206-016-0205-7

A novel prediction method of vibration and acoustic radiation for rectangular plate with particle dampers †

Dongqiang Wang[1] and Chengjun Wu[1,2,*]

[1]*School of Mechanical Engineering, Xi'an Jiaotong University, Xi'an 710049, China*
[2]*State Key Laboratory for Strength and Vibration of Mechanical Structures, Xi'an Jiaotong University, Xi'an 710049, China*

(Manuscript Received April 22, 2015; Revised October 18, 2015; Accepted November 17, 2015)

Abstract

Particle damping technology is widely used in mechanical and structural systems or civil engineering to reduce vibration and suppress noise as a result of its high efficiency, simplicity and easy implementation, low cost, and energy-saving characteristic without the need for any auxiliary power equipment. Research on particle damping theory has focused on the vibration response of the particle damping structure, but the acoustic radiation of the particle damping structure is rarely investigated. Therefore, a feasible modeling method to predict the vibration response and acoustic radiation of the particle damping structure is desirable to satisfy the actual requirements in industrial practice. In this paper, a novel simulation method based on multiphase flow theory of gas particle by COMSOL multiphysics is developed to study the vibration and acoustic radiation characteristics of a cantilever rectangular plate with Particle dampers (PDs). The frequency response functions and scattered far-field sound pressure level of the plate without and with PDs under forced vibration are predicted, and the predictions agree well with the experimental results. Results demonstrate that the added PDs have a significant effect on vibration damping and noise reduction for the primary structure. The presented work in this paper shows that the theoretical work is valid, which can provide important theoretical guidance for low-noise optimization design of particle damping structure. This model also has an important reference value for the noise control of this kind of structure.

Keywords: Particle damping technology; Vibration response; Acoustic radiation; Multiphase flow theory

1. Introduction

Particle damping is a promising technique of providing damping with granular metal particles filled within a relatively simple auxiliary enclosure called Particle damper (PD), which is attached to a vibrating structure [1, 2]. The particles dissipate energy through particle-to-wall and particle-particle friction and collisions. Energy is mostly dissipated as heat and noise, together with the development of high-frequency vibrations in the structure. Particle damping is regarded an alternative of traditional passive damping methods because of its extreme simplicity without the need for any auxiliary power equipment, high effectiveness, low cost, and ability to operate in adverse working conditions compared with the forms of viscoelastic materials, frictional devices, tuned absorbers, and isolators [3, 4]. Although PD is a derivative of a single unit impact damper referred to as impact damper, it has a tremendous potential for noise reduction and vibration attenuation in a broad frequency range compared with impact damper.

Particle damping has been investigated over the past decades [1, 5, 6]. It has been successfully used to satisfy the vibration attenuation of steam turbine buckets [7], printing cylinders [8], rotating blades [9], vehicles [10], radar antenna [11], and machine tools [12]. However, particle damping theory significantly lags behind the development of techniques for vibration control, particularly for noise reduction. Most particle damping research has been focused on experimental research rather than theoretical research for analytical models of particle damping. Recently, several approaches have been proven useful and available for predicting the vibration characteristics of particle damping structures. The lumped mass approach [13-19] and Discrete element method (DEM) [5, 20-27] are used to predict the corresponding dynamic response of the particle damping structure. Nevertheless, the above application fields are only limited to the Single-degree-of-freedom (SDOF) system or equivalent SDOF. In addition to the above methods, recent researchers have performed limited studies to evaluate the dissipative properties of granular materials based on multiphase flow theory of gas particle mathematically [28, 29]. This new modeling approach is promising because it offers the possibility of capturing the physics nature of granular damping using an analytical perspective with considerably

*Corresponding author. Tel.: +86 29 82668573, Fax.: +86 29 83237910
E-mail address: 445wdq@163.com
† Recommended by Associate Editor Junhong Park

reduced complexity analysis and computational cost [29]. Wu et al. [30, 31] further developed the original mathematical model based on the previous work [28, 29] to improve the forecast accuracy of the model; in this model, particle damping is equivalent to the viscous damping, including interparticle collision and friction effects using multiphase flow theory of gas particle. The predictions of the improved model are compared with the results from the original model for appropriate mass packing ratios and excitation levels. Numerical results showed that the predictions of the improved model agree fairly well with the experimental results in Ref. [28] and DEM simulations in Ref. [29]. Wang et al. [32] further applied the improved model to predict the dynamic responses of the continuum particle damping composite structure (i.e., a cantilever beam with PD under forced vibration). Furthermore, experimental verifications were performed. Good correlations were obtained between the analytical results and experimental data. Although several approaches have been proven useful and available for predicting the particle damping performance, these previous studies were all limited to the prediction of vibration response; they were rarely involved in the prediction of structural acoustic radiation for the continuous particle damping structure in the existing literature.

This paper aims to bring attention to particle damping theory not only for the prediction of both the vibration response and structural acoustic radiation. Our task is to develop a feasible simulation method using multiphase flow theory of gas particle via a self-developed analysis model combined with a COMSOL Multiphysics model to predict the response of acoustic vibration for the continuous particle damping structure based on the previous work of Wang et al. [32, 33].

The present study consists of theoretical research, numerical prediction, and experimental verification. Sec. 2 provides a detailed introduction to the development of our theoretical model. Sec. 3 presents our research plan and explains the process and simulation results. In Sec. 4, a forced vibration experiment of the cantilever rectangular plate with and without PDs is conducted by comparing the results of numerical simulation and experiment to verify the model. Finally, conclusions are given in Sec. 5.

2. Basic theory

As mentioned in Ref. [34], the granular particles enclosed in a cavity of a vibrating structure can be considered a multiphase flow of gas particle with low Reynolds number, in which the particle concentration is high (i.e., the flow is dense).

2.1 Model development

For inelastic particles and a simple shear flow, such as a laminar flow, the effective viscosity caused by interparticle collisions can be derived from kinetic theory of dense multiphase flow as follows [34]:

$$\mu_c=\frac{6}{5}(1+e_p)\sqrt{\frac{\Theta}{\pi}}\alpha_p{}^2 g_p\rho_p d_p \tag{1}$$

where

$$g_p=\frac{1}{1-\alpha_p}+\frac{3\alpha_p}{2(1-\alpha_p)^2}+\frac{\alpha_p{}^2}{2(1-\alpha_p)^3}. \tag{2}$$

The equivalent shear viscosity corresponding to the friction force between particles can be expressed as follows [35]:

$$\mu_f=\frac{p_p\sin\phi}{2\sqrt{I_{2D}}} \tag{3}$$

where p_p is the solid pressure, which is composed of a kinetic term and a second term caused by particle collision [36]:

$$p_p=\alpha_p\rho_p\Theta+2\rho_p(1+e_p)g_p\alpha_p{}^2\Theta. \tag{4}$$

The fluctuation-specific kinetic energy is $\Theta=\langle\dot{x}^2\rangle/3$. For harmonic motion $\langle\dot{x}^2\rangle=|\dot{x}|^2/2$, Eq. (1) can be rewritten as follows:

$$\mu_c=\frac{1}{5}(1+e_p)\sqrt{\frac{6}{\pi}}\alpha_p{}^2 g_p\rho_p d_p|\dot{x}| \tag{5}$$

with

$$K_1=\frac{1}{5}\sqrt{\frac{6}{\pi}}(1+e_p)\alpha_p{}^2 g_p\rho_p d_p \tag{6}$$

where

$$\mu_c=K_1|\dot{x}|. \tag{7}$$

Inserting Eq. (4) into Eq. (3), Eq. (3) can be rewritten as follows:

$$\mu_f=\frac{(\alpha_p\rho_p+2\rho_p(1+e_p)g_p\alpha_p{}^2)\sin\phi}{12\sqrt{I_{2D}}}|\dot{x}|^2 \tag{8}$$

with

$$K_2=\frac{(\alpha_p\rho_p+2\rho_p(1+e_p)g_p\alpha_p{}^2)\sin\phi}{12\sqrt{I_{2D}}} \tag{9}$$

where

$$\mu_f=K_2|\dot{x}|^2. \tag{10}$$

Considering that the friction and collision models have the same form of expression based on multiphase flow theory of

gas particle, the complete damping effect between particles can be uniformly expressed as follows:

$$\mu_p = K_1|\dot{x}| + K_2|\dot{x}|^2 . \tag{11}$$

Furthermore, the viscosity of the gas particle mixture flow is $\mu_m = \mu_p + \mu_g$. Generally, $\mu_p \gg \mu_g$, then $\mu_m \approx \mu_p$. The drag force $F_{d,viscous}$ of the equivalent viscous damping can be formulated as follows [37]:

$$F_{d,viscous} = -\frac{1}{2}\rho_m S C_d |\dot{x}|\dot{x} = -C_{eq}\dot{x} \tag{12}$$

where $\dot{x}$ is the vibration velocity of the plate where the PDs are added (i.e., the velocity of cavity).

$$C_{eq} = \frac{1}{2}\rho_m S C_d |\dot{x}| \tag{13}$$

where C_{eq} represents the equivalent nonlinear viscous damping caused by the effects of collisions and friction between the particles enclosed in a cavity of a vibrating structure, $S=dh$ is the lengthwise section area of the cavity, and the drag coefficient C_d is given by Sarpkaya [38]:

$$C_d = \frac{fd\pi^3}{|\dot{x}|}\left(\frac{3}{2}\beta^{-1/2} + \frac{3}{2}\beta^{-1} - \frac{3}{8}\beta^{-3/2}\right) \tag{14}$$

where $\beta = \pi d^2 f \rho_m / \mu_p$; inserting Eq. (11) into Eq. (14), Eq. (14) can be rewritten as follows:

$$C_d = \frac{fd\pi^3}{|\dot{x}|}\left[\frac{3}{2}\left(\frac{K_1|\dot{x}| + K_2|\dot{x}|^2}{\pi d^2 f \rho_m}\right)^{1/2} + \frac{3}{2}\left(\frac{K_1|\dot{x}| + K_2|\dot{x}|^2}{\pi d^2 f \rho_m}\right)^{1} - \frac{3}{8}\left(\frac{K_1|\dot{x}| + K_2|\dot{x}|^2}{\pi d^2 f \rho_m}\right)^{3/2}\right] \tag{15}$$

inserting Eq. (15) into Eq. (13) via some mathematical manipulations, the model expression of the equivalent nonlinear viscous damping has a uniform expression because of the effects of interparticle collisions and friction as the following forms:

$$\begin{aligned} C_{eq} = {} & \frac{3\pi^3 d^2 h \rho_m}{4}\left(\frac{K_1}{\pi d^2 \rho_m}\right)^{1/2} f^{1/2}|\dot{x}|^{1/2} + \frac{3\pi^3 d^2 h \rho_m}{4}\left(\frac{K_1}{\pi d^2 \rho_m}\right)|\dot{x}| \\ & - \frac{3\pi^3 d^2 h \rho_m}{16}\left(\frac{K_1}{\pi d^2 \rho_m}\right)^{3/2} f^{-1/2}|\dot{x}|^{2/3} + \frac{3\pi^3 d^2 h \rho_m}{4}\left(\frac{K_2}{\pi d^2 \rho_m}\right)^{1/2}|\dot{x}| \\ & + \frac{3\pi^3 d^2 h \rho_m}{4}\left(\frac{K_2}{\pi d^2 \rho_m}\right)|\dot{x}|^2 - \frac{3\pi^3 d^2 h \rho_m}{16}\left(\frac{K_2}{\pi d^2 \rho_m}\right)^{3/2} f^{-1/2}|\dot{x}|^3 . \end{aligned} \tag{16}$$

The equivalent viscous damping caused by interparticle friction and collisions for the gas particle mixture flow in a cavity of a vibrating structure is a kind of high nonlinear damping related to the velocity amplitude of the vibrating structure (Eq. (16)).

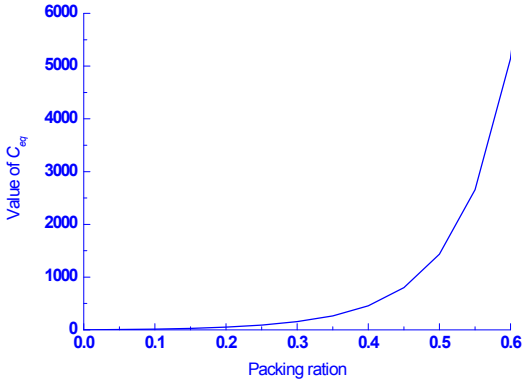

Fig. 1. Curve of the equivalent damping coefficient C_{eq} versus the packing ration α_p.

2.2 Parametric analysis

From the mathematical expressions of Eq. (16), C_{eq} is the multiple parameter function. The change in any parameter value will alter the values of C_{eq} (such as e_p restitution coefficient of the particle, α_p packing ratio, ρ_p density of particle, d_p mean diameter of particles, d inside diameter of the cavity, and h height of the cavity). Based on Eqs. (6) and (9), the K_1 value is proportional to the above parameters e_p, α_p, ρ_p and d_p; the K_2 value is proportional to the above parameters e_p, α_p and ρ_p. The K_1 and K_2 parameters have no actual physical meaning in the article; these parameters are intermediate variables produced in the formula deduction process to shorten the length of Eq. (16).

Generally, the value range of e_p is from 0 to 1; the value range of α_p is from 0 to 0.63 [18]; and the value range of d_p is from 0.05 to 0.5 (mm) [15]. Nominally, the ρ_p value range can be any value. We mainly discuss the influence of α_p, e_p, d_p and ρ_p on the value of C_{eq}. Change in cavity size means mass packing change. For cavity size, this case is not further discussed. To facilitate this discussion, the abovementioned parameters are assumed to be dimensionless. When one of the parameters is discussed, the values of other parameters are selected from Table 1 and maintained constant. We assume that the amplitude of vibration velocity $|\dot{x}|$ and frequency are 0.5 and 20, respectively. The curves of C_{eq} versus α_p, e_p, d_p and ρ_p are as follows:

Figs. 1 and 3 show that C_{eq} increases with the increase in packing ration and diameter of particle; however, the damping coefficient shows nonlinear characteristics. When the packing ration is more than 40%, the nonlinear characteristics are more obvious, and the increase in the value is more intense. By contrast, the damping coefficient increases linearly with the increase in density and restitution coefficient of particle from Figs. 2 and 4. The density of particle has a greater contribution to damping than the restitution coefficient of particle.

Table 1. Coordinates of the Particle dampers (PDs), measurement points, and excitation point (mm).

Item	Number and coordinate			
Measurement point	Point 1	Point 2	Point 3	Point 4
	(300, 80, 0)	(300, 0, 0)	(300, −80, 0)	(210, 80, 0)
	Point 5	Point 6	Point 7	Point 8
	(210, 0, 0)	(210, −80, 0)	(120, 80, 0)	(120, 0, 0)
	Point 9	Point 10	Point 11	Point 12
	(120, −80, 0)	(30, 80, 0)	(30, 0, 0)	(30, −80, 0)
PDs	Damper A	Damper B	Damper C	Damper D
	(270, 0, 0)	(210, 80, 0)	(210, −80, 0)	(90, 0, 0)
Excitation point	(275, 0, −6)			

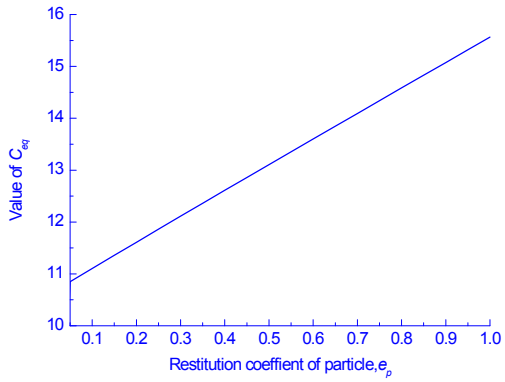

Fig. 2. Curve of the equivalent damping coefficient C_{eq} versus the restitution coefficient of particle e_p .

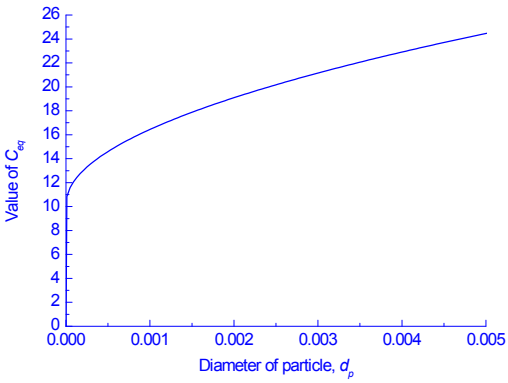

Fig. 3. Curve of the equivalent damping coefficient C_{eq} versus the diameter of particle d_p .

Density and high packing of particle ratio significantly influence damping performance in vibration attenuation [18, 28, 39], which is in accordance with the research conclusion of this article.

From the mathematical expressions of Eq. (16), the level of the equivalent damping coefficient C_{eq} is highly nonlinear (i.e., the amplitude of vibration velocity). Hence, we further discuss the influence of the amplitude of vibration velocity $|\dot{x}|$ on the level of damping coefficient C_{eq} ; other parameters are selected from Table 2 and maintained constant.

Table 2. Characteristics and properties of the plate, PD and particle used in the model.

Item	Characteristics and properties				
Plate	Material	Young's modulus (Pa)	Density (kg/m^3)	Poisson ratio	Length (mm)
	Aluminum alloy	5.6×10^{10}	2646	0.27	300
	Width (mm)	Thickness (mm)			
	200	6			
PD	Material	Weight (g)	Inside diameter (mm)	Outside diameter (mm)	Height (mm)
	Aluminum alloy	14.52	16	20	20
Particle	Material	Density (kg/m^3)	Restitution coefficient	Kinetic friction coefficient	
	Tungsten powder	17000	0.6	0.3	

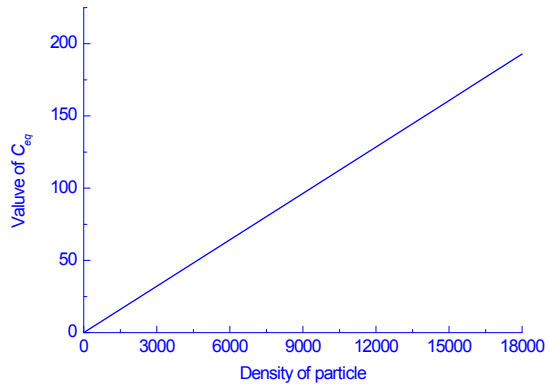

Fig. 4. Curve of the equivalent damping coefficient C_{eq} versus the density of particle ρ_p .

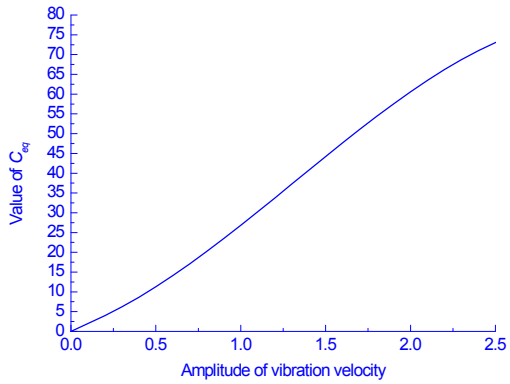

Fig. 5. Curve of the equivalent damping coefficient C_{eq} versus the amplitude of vibration velocity density of particle $|\dot{x}|$.

Fig. 5 shows that the value of the equivalent damping coefficient C_{eq} exhibits nonlinear characteristics; it increases with the increase in the amplitude of vibration velocity (i.e., excitation amplitude-dependent).

In fact, the topic of the above discussion is a multiple-

parameter optimization problem. Determining which term is most important with the level of contribution to the damping coefficient is difficult. If one of the abovementioned parameters is discussed, the values of other parameters remain constant (Table 2). Based on Figs. 1-4, the contribution of the packing ration to the reduction of the vibration is the highest among them.

Moreover, the damping performance of the whole system, including the plate and PDs, is closely related to the above parameters, as well as the dimension and material of the enclosure, placement position of the PDS, level of acceleration of the primary structure, and excitation frequency [40].

Many researchers have concluded that particle damping is highly nonlinear [15, 28, 29, 41]. To obtain the optimum damping effect, the different combinations of system parameters should be optimized.

Considering only a single factor, brute force methods (full sorting) may be available; however, full sorting is not competent for the many parameters above or many inputs and outputs [42]. Simonian stated that when forced vibration is concerned, the resulting damping performance depends on vibration amplitude and mass packing ratio [3]. In forced vibration applications, an optimum mass packing ratio exists for a given vibration amplitude. Parameter optimization is necessary to obtain a good damping effect for the different combinations of system parameters in our next work.

2.3 Vibration response

For the continuous particle damping structure, the PD contribution is estimated as an equivalent spring mass system; nevertheless, the system does not exhibit any stiffness (i.e., mass damping system). The damping coefficient of the mass damping system responds to the equivalent nonlinear viscous damping coefficient C_{eq} (Eq. (16)) determined for different levels of excitation and depending on the excitation velocity amplitude. The mas of the mass damping system responds to the equivalent total mass M_{eq}, which includes the mass of the enclosure and total mass of particles filled.

A simple cantilever plate with PDs is considered an attempt to validate the theory in this paper. Fig. 6 shows a sketch of the considered plate with the PDs, as well as the adopted model.

The plate is modeled by finite element method using the discrete Kirchhoff quadrilateral element. The motion of the global system is governed by the following equation:

$$\mathbf{M}\cdot\ddot{\mathbf{X}}+\mathbf{C}\cdot\dot{\mathbf{X}}+\mathbf{K}\cdot\mathbf{X}=\mathbf{F}. \tag{17}$$

2.4 Acoustic radiation

For the acoustic-solid interaction, the boundary condition includes the following interaction from solid to gas and vice versa: to couple the acoustic pressure wave to the solid wall, the boundary load $\mathbf{P}$ (force/unit area) on the wall is set to

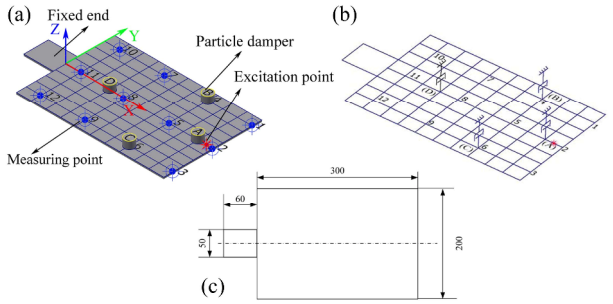

Fig. 6. Sketch of the cantilever plate dimension and PD arrangement.

the following:

$$\mathbf{P}=-\mathbf{n}_s p. \tag{18}$$

The structural acceleration acting on the boundaries between the solid and gas causes the normal acceleration for the acoustic pressure on the boundary equal to the acceleration based on the second derivatives of the structural displacements $\mathbf{u}$ with respect to time: $a_n=\mathbf{n}_a\cdot\omega^2\mathbf{u}$.

To couple back the frequency response of the solid to the acoustics problem, a normal acceleration boundary condition is used, setting the normal acceleration a_n to $\left(\mathbf{n}_a\cdot\mathbf{u}\right)\cdot\omega^2$.

$$-\mathbf{n}_\alpha\cdot\left(-\frac{1}{p_o}\nabla p+\mathbf{q}\right)=a_n. \tag{19}$$

Notably, the simulation is conducted via COMSOL Multiphysics software. This software is a multiphysics coupling software with powerful processing capacity; it is a flexible platform that allows users to enter coupled systems of Partial differential equations (PDEs). PDEs can be entered directly or using the so-called weak form. In the simulation, COMSOL Multiphysics software provides a simulation option for the spring-mass-damper system with access to self-programming. Thus, the equivalent viscous damping, including the interparticle collisions and friction effects, can be embedded into COMSOL Multiphysics software. Such an idea is novel and leads to a new breakthrough because it offers the possibility to predict the vibration response and acoustic radiation of complicated continuous structures with PDs in finite element method via COMSOL; this model has reduced complexity analysis and computational cost. Once the geometric parameters, physical parameters, and boundary conditions of the structure in simulation are set, the prediction of acoustic and vibration of a cantilever rectangular plate with PDs should be implemented by COMSOL.

3. Numerical simulation

To validate the theory developed in this paper and evaluate the vibration response and acoustic radiation of a cantilever rectangular plate with PDs under forced excitation, the process

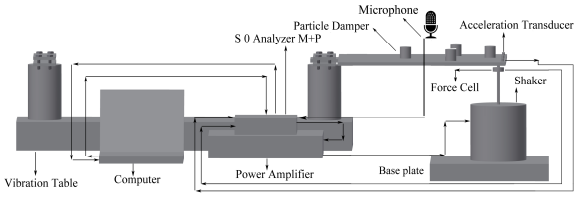

Fig. 7. Schematic of experimental setup.

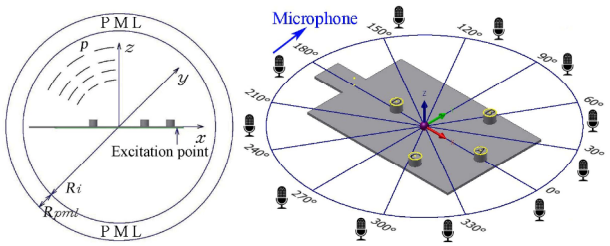

(a) (b)

Fig. 8. (a) Sketch of the modeled system; (b) microphone layout in the *x*-*y* plane.

of numerical simulation is organized in two steps.

In the first step, the original plate without PD is first tested to characterize the dynamic behavior and acoustic radiation characteristics of the primary structure. This set of tests aims to verify the geometric model, load, and boundary condition applied, which includes the analysis and calibration of the experiment parameters that have an effect on the measurement precision.

In the second step, vibration responses and acoustic radiation of the plate with PDs are investigated to reveal the damping effect of the PDs. For comparison, the excitation level, excitation location, and measurement points are the same as the test used in the above step. Fig. 6 shows the positions of observation points, PDs, and excitation point on the plates. Table 1 presents the coordinates of the PDs, measurement points and excitation point.

The exciter is attached to the bottom of the plate using the adhesive, which provides harmonic force to the structure (Fig. 7). The harmonic force, $F = A\sin(\omega t)$ can be set by the SO M+P Analyzer system; the excitation signal through the power amplifier is transferred to the exciter.

A total of 12 measurement points are on the top of the plate (Fig. 6). Table 2 provides a list of the characteristics and properties of the plate, PD and particles used in the model.

The microphones are in the *x*-*y* plane, which are flush with the tops of the plate. Fig. 8(b) shows the detailed layout of the microphones. The microphones are evenly arranged on the circumference of a circle with the interval of 30° in the *x*-*y* plane; the circle has a radius of 1000 mm.

Fig. 8(a) depicts the sketch of the acoustic modeled system. The entire system (the plate with PDs) is located inside a computational domain with a total radius $R_i + R_{pml}$, where R_i = 400 mm and R_{pml} = 80 mm. The layer of thickness R_{pml} is the absorbing Perfectly matched layer (PML), which is indicated in Fig. 8(a). PML is used as a non-reflecting and absorbing boundary, which mimics a domain stretching to infinity. The scattered field is denoted as p.

Our particle damping method uses four enclosures filled with tungsten particles of small size, which are attached to the primary structure (the cantilever rectangular plate). The mass packing ratio in every damper is 50%. The mass packing ratio α_{mp}, which is defined as the actual packing mass of particles to the maximum permissive packing mass of particles in a cavity, is introduced to describe the packing condition of the damper. The particle mass of each filled PD is 11.60×10^{3} kg.

Twelve points distributed uniformly on the plates are used as the observation points to acquire the vibration response of the plate adequately and study the dynamic characteristics of the structure under forced excitation. Four PDs are symmetrically attached to the plate to obtain an ideal damping effect and avoid the effects that the asymmetry of the additional mass brings to the structure. The handle part in the figure refers to the fixed end of the plate (Fig. 6).

After building the geometric model of the plate, the parameters of material properties, including density, Young's modulus, and Poisson's ratio of the plate, are set in COMSOL. The physical constraints are applied on the plates, including fixed end, structural damping, mass of the dampers, and equivalent viscous damping caused by interparticle collision and friction effects. The range of the frequency of sine excitation is from 0 Hz to 800 Hz, with an interval of 2 Hz.

3.1 Vibration response prediction

The Frequency response functions (FRFs) of the plate are successively measured; these functions are the ratio of acceleration amplitude to the excitation force on each observation point. The curve of the FRFs is used to evaluate the vibration intensity of the plate. Notably, the value of the equivalent damping coefficient depends on the excitation amplitudes (Eq. (16)). We only consider FRFs to evaluate the level of vibration without considering the excitation amplitudes. In the experimental process, when the excitation frequency is close to the resonance frequency of the system, the excitation force will increase; when the excitation frequency is away from the resonance frequency of the system, the excitation force will decrease. The excitation force changes with the increase in excitation frequency, which is not a constant value. Thus, an exact expression for the function of excitation force is difficult to obtain.

In the simulation process, if the input force (excitation force) cannot be given accurately, simulation cannot be calculated. The acceleration response of the whole system cannot also be obtained. We cannot compare the simulation results and experimental data, as well as assess the correctness of the model. For the forced vibration system, we evaluate the level of vibration not only from the velocity response and acceleration response but also from the FRFs. For example, when the system is subjected to harmonic vibration, the motion of the

global system is governed by the following equation:

$$\mathbf{M}\cdot\ddot{\mathbf{X}}+\mathbf{C}\cdot\dot{\mathbf{X}}+\mathbf{K}\cdot\mathbf{X}=\mathbf{F}$$

where $\mathbf{F}=\mathbf{P}\sin\omega t$ is a harmonic excitation force, and $\mathbf{P}$ is an excitation amplitude. Laplace transform is used in Eq. (17); subsequently, we can obtain the transfer function of the whole system as follows:

$$\left(\mathbf{M}s^2+\mathbf{C}s+\mathbf{K}\right)\mathbf{X}(s)=\mathbf{P}(s) \tag{20}$$

$$G(s)=\frac{\mathbf{X}(s)}{\mathbf{P}(s)}=\frac{1}{\mathbf{M}s^2+\mathbf{C}s+\mathbf{K}} \tag{21}$$

where $G(s)$ is the transfer function and a complex variable. With $s=i\omega$, $H(\omega)=G(s)\big|_{s=i\omega}$, we can obtain the displacement response in the frequency domain:

$$\mathbf{X}(\omega)=\mathbf{P}(\omega)H(\omega). \tag{22}$$

The acceleration response in the frequency domain is as follows:

$$\ddot{\mathbf{X}}(\omega)=\mathbf{P}(\omega)H_a(\omega). \tag{23}$$

Eq. (23) shows that the level of the acceleration response depends on the excitation amplitudes. We can easily obtain the acceleration response function in the frequency domain (i.e., FRFs):

$$H_a(\omega)=\frac{\ddot{\mathbf{X}}(\omega)}{\mathbf{P}(\omega)}=\frac{-\omega^2}{\mathbf{K}-\mathbf{M}\omega^2+i\omega\mathbf{C}}. \tag{24}$$

This article aims to verify the model developed to predict the vibration response and acoustic radiation of the particle damping structure based on multiphase flow theory of gas particle. We do not only consider the simulation result but also the experimental data for comparisons. In the simulation process, if the system is applied a unit harmonic vibration, we may obtain FRFs. Therefore, the FRFs (acceleration /force) of the rectangular plate with PD are used to describe the damping effect and verify the validity of the model in this article for the sake of convenience for comparative analysis between simulation results and experimental data. Moreover, we do not consider the contribution of the excitation amplitude.

Other researchers also used FRFs to present the characteristics of particle damping. Trigui et al. used FRFs to show the influence of the two configurations of PD positions on vibration attenuation [40]. Veeramuthuvel et al. [43] used FRFs to present the influence of different packing rations and granular materials on the damping effect.

Any four points at the plate can then be used as observation points to display the vibration response of the whole plate; these points are points 2, 6, 8 and 11.

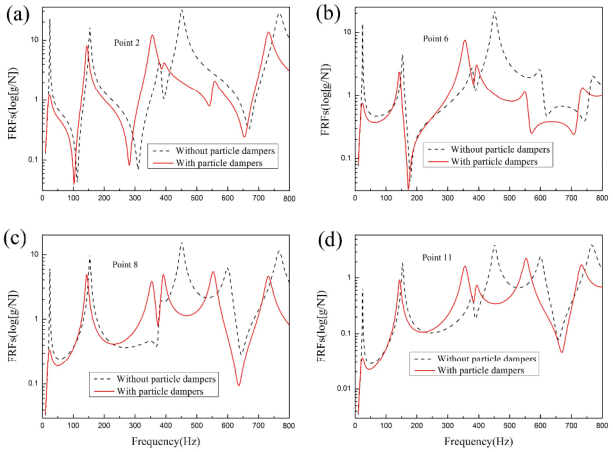

Fig. 9. Simulation result comparison of the Frequency response functions (FRFs) on the rectangular plate with and without PDs.

Fig. 9 shows that the acceleration amplitude of each point declines obviously after the PDs are exerted on the plates at a number of resonance frequencies over a certain band of frequencies. The presence of PDs causes an increase in modal damping, thereby suggesting that PDs are highly efficient for the plate-like structure to suppress vibration from the use of a minimal quantity of particles. The rate of the total particle mass (34.8 g) to the primary structure mass (1 kg) is only 3.5%. Particle damping exhibits a reduction in the response amplitude by 87.5% from the vibration amplitude of the first-order natural frequency in Fig. 9(a). The damping effect is also high and remarkable in the whole frequency range, which allows us to investigate the broadband effect of particle damping.

In Fig. 9, natural frequencies shift to the left in the FRF curves when the PDs are exerted on the plate compared with the case of the plate without PDs. This phenomenon is specifically obvious within the frequency range of 300-800 Hz because the added PDs change the mass matrix of the whole system. However, the particle damping effect can reach relatively high levels for the first- and second-order modes of the plate without significant changes in the natural frequencies and mode shapes compared with the case of the plate without PDs. This result indicates that particle damping technology shows a small effect on the natural frequencies and mode shape for the low-order model. In addition, the original plate (without the PDs) has a high level of response, specifically within the frequency ranges of 0-50 and 400-550 Hz. The particle damping treatment of the plate causes a significant improvement in reducing the vibration response, whereas the vibration reduction in the lower range of 200-300 Hz is modest. This result shows that this particular treatment of the plate may have some trade-offs.

Fig. 9 also shows that the vibration mode around 470 Hz is more energetic than the fundamental mode. Through the

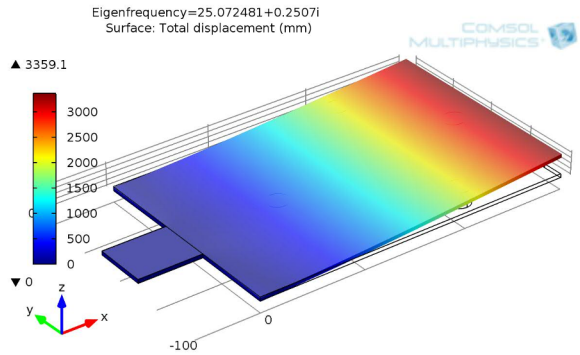

Fig. 10. Vibration mode shape of the cantilever rectangular plate without PDs under the first order of natural frequency.

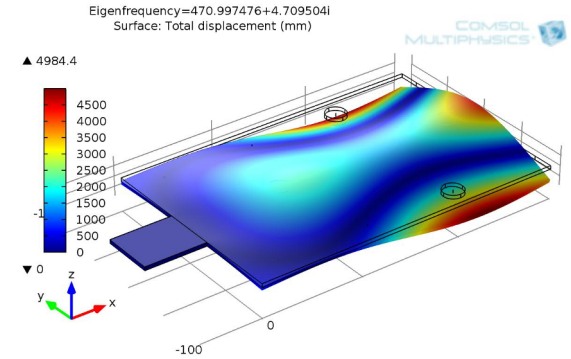

Fig. 11. Vibration mode shape of the cantilever rectangular plate without PDs under the fourth order of natural frequency.

analysis of the eigenfrequencies of the cantilever rectangular plate without PDs, the first and fourth orders of natural frequencies along the *z*-direction are obtained, which are 25 and 470 Hz, respectively. Figs. 10 and 11 present the longitudinal vibration mode shapes of the first and fourth orders of natural frequencies.

When the excitation frequency is equal to the fourth natural frequency, we find that the vibration amplitudes of the rectangular plate at measuring points 2, 6, 8 and 11 are higher than the case of the first natural frequency from the range value of color legend in Figs. 10 and 11 through the analysis of modal frequencies and mode shapes. For a better view of the comparison, the data of the acceleration amplitude are retrieved from the same observation points on the rectangular plate without PDs in different natural frequencies. The vibration mode around 470 Hz is more energetic than the fundamental mode (Fig. 12). The vibration amplitude at measurement points is related to mode shapes. Similar phenomenon can also be observed from Fig. 9 when the plate has PDs, which may originate from the same reason.

3.2 Acoustic radiation prediction

3.2.1 Sound pressure level (SPL)

Figs. 13 and 16 show that the model calculates the frequency response from the solid and subsequently feeds this

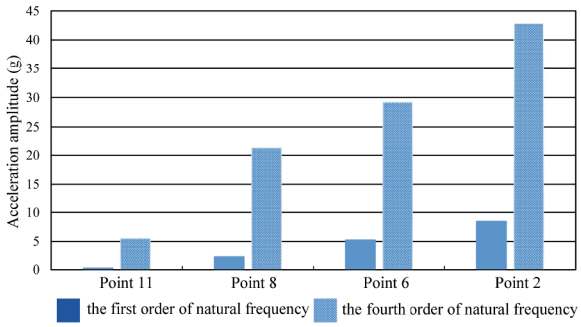

Fig. 12. Comparison of the acceleration amplitude at the same observation point on the rectangular plate under different natural frequencies.

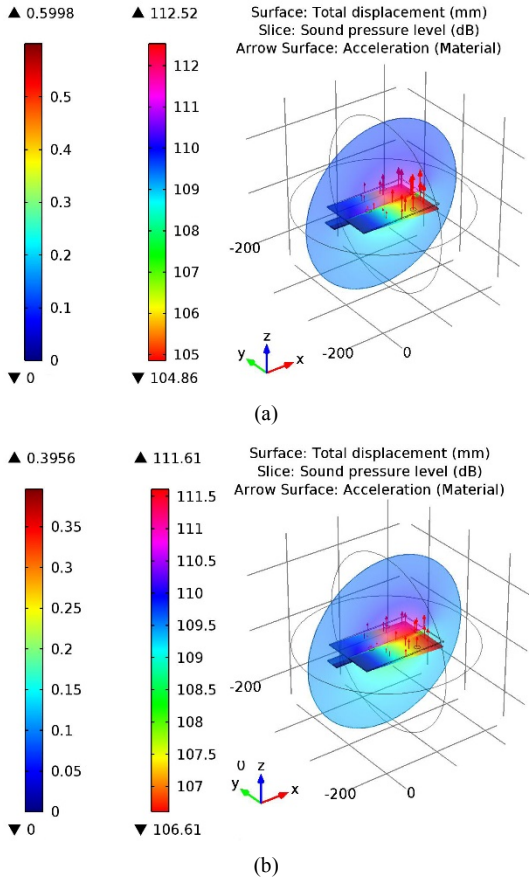

Fig. 13. (a) Sound-pressure plot (dB) of the acoustic waves in the coupled problem at f = 50 Hz for the plate without PDs; (b) sound-pressure plot (dB) of the acoustic waves in the coupled problem at f = 50 Hz for the plate with PDs.

information back to the acoustics domain so that it can analyze the wave pattern. The air acoustic domain is truncated as a sphere with a reasonably large diameter, which depends on the performance of the computer. Four frequencies, namely, 50, 150, 400 and 600 Hz, are investigated for the plate with and without PDs.

Figs. 13 and 16 display the sound pressure as a slice plot. These figures clearly show from which direction the accelera-

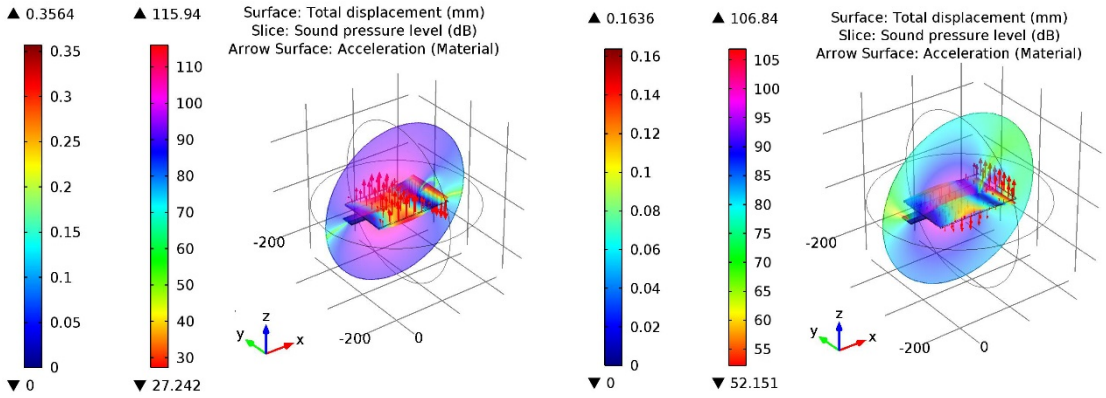

(a) (b)

Fig. 14. (a) Sound-pressure plot (dB) of the acoustic waves in the coupled problem at f = 150 Hz for the plate without PDs; (b) sound-pressure plot (dB) of the acoustic waves in the coupled problem at f = 150 Hz for the plate with PDs.

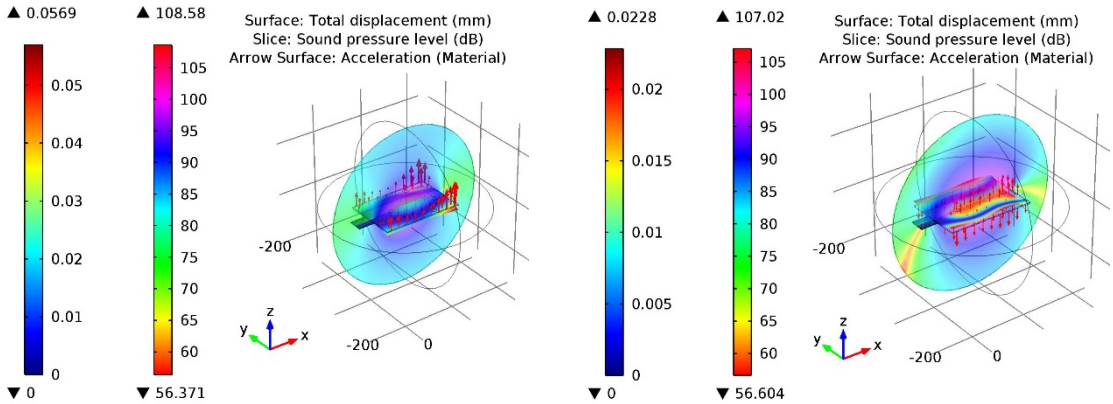

(a) (b)

Fig. 15. (a) Sound-pressure plot (dB) of the acoustic waves in the coupled problem at f = 400 Hz for the plate without PDs; (b) sound-pressure plot (dB) of the acoustic waves in the coupled problem at f = 400 Hz for the plate with PDs.

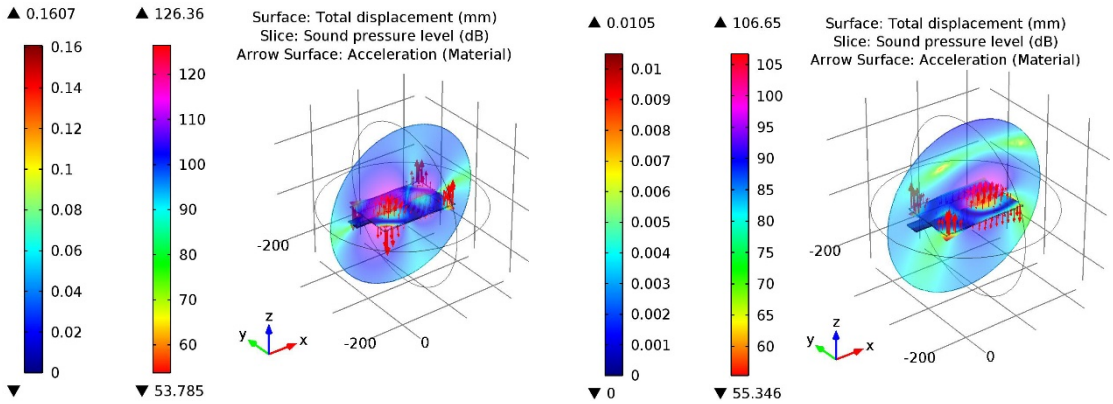

(a) (b)

Fig. 16. (a) Sound-pressure plot (dB) of the acoustic waves in the coupled problem at f = 600 Hz for the plate without PDs; (b) sound-pressure plot (dB) of the acoustic waves in the coupled problem at f = 600 Hz for the plate with PDs.

tion propagates into the air domain. The values of deformation are very small, but the acceleration is sufficiently large to influence the sound waves. The arrow lengths are proportional to the surface acceleration, which is a direct measure of the sound-pressure interaction between the air and plate. By contrast, with the same imposed vibration under identical frequen-

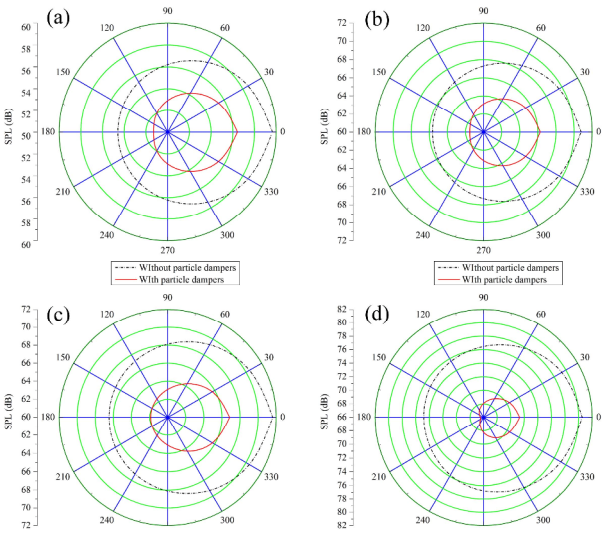

Fig. 17. Comparison of the far-field Sound pressure level (SPL) of the plate with and without PDs at a radius of 1000 mm in the *x-y* plane.

cies, the plate with PDs presents a better damping effect compared with that without PDs, regardless of the overall sound pressure level or normal acceleration of the solid surface.

3.2.2 Far-field SPL

Using the far-field calculation feature, SPL in the scattered field at a given distance outside the computational domain is used to reflect the acoustic radiation ability of the plate. The plate is excited by a sinusoidal mechanical boundary load on the bottom surface of the plate and at a frequency specified in the study: 50, 150, 400 and 600 Hz. The far-field SPL outside the modeling domain at a radius of 1000 mm in the *x-y* plane is calculated. Fig. 17 depicts the SPL distribution at 50, 150, 400, and 600 Hz. The result is presented as 2D plot groups and polar plots of the scattered far-field SPL. The data are retrieved in the *x-y* plane and presented as a polar plot, with 0° corresponding to the positive *x*-direction (Fig. 8(b)).

Figs. 17(a)-(d) demonstrate that the scattered acoustic pressure performance may be effectively improved by the added PDs. The results also indicate that the sound field has obvious symmetry; the SPL in the head of the model plate is bigger than that of the tail of the model plate. This phenomenon may be caused by the excitation location, which is close to the front of the plate.

Table 3 illustrates that the SPL value on the circumference of a radius of 1000 mm in the *x-y* plane in Fig. 17 indicates a mean value. The average rate of decrease in the SPL value of the plate with PDs to the value of the plate without PDs is as high as 11.45% in the excitation frequency of 600 Hz. This result confirms that the acoustic radiation characteristic of the particle damping structure is sensitive to the excitation frequency. This result also reveals that the mode shape of the structure has a fairly significant effect on acoustic radiation modes.

Table 3. SPL mean value of simulation in the far-field at a radius of 1000 mm in the *x-y* plane when the plate is with and without PD.

Excitation frequency (Hz)	Mean value (dB)		Amount of reduction (dB)	Rate decrease
	Without PDs	With PDs		
50	57.07	53.72	3.35	5.87%
200	68.19	63.83	4.36	6.39%
400	69.03	64.06	4.97	7.20%
600	77.72	68.82	8.9	11.45%

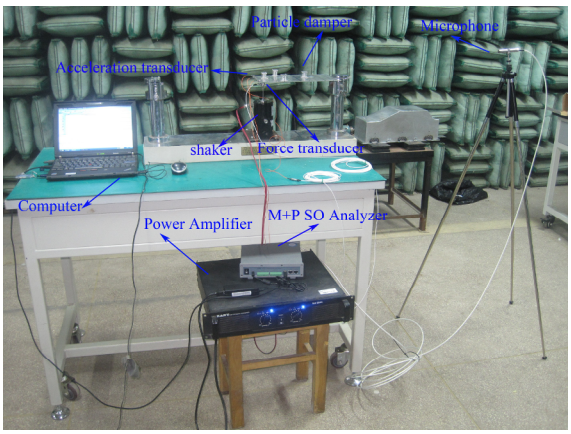

Fig. 18. Picture of the experimental apparatus used.

4. Experiment verification

To verify the theoretical model developed in this study, an experiment for the cantilever rectangular plate with and without PDs is set up. The specifications for the experiment are maintained the same as those in the simulation for comparison. Fig. 18 presents a picture of the experimental apparatus used.

4.1 Vibration response verification

The experimental model consists of the primary structure (cantilever rectangular plate) and four aluminum enclosures containing tungsten particles. The enclosures are partially filled with tungsten particles, which are attached to the top of the rectangular plate that is itself attached to an electromagnetic shaker (MB MODAL 50A), providing an excitation force. The signal of the harmonic excitation amplified by power amplifier (M B500VI) is transferred to the shaker. A microphone (Dytran 40AE/26CA) is used to measure the far-field sound pressure. The force and acceleration signals are measured with a force transducer (Dytran1051V4) and acceleration transducer (Dytran 3133B1), both with a mass of 0.6 g. A dynamic signal analyzer (M+P SO Analyzer) made in Germany is used to collect and process the data. The whole process is tested in a semi-anechoic room.

In this experiment, the frequency range of sine sweep excitation is 2-800 Hz, and the frequency step is 2 Hz. The sweep rate is 300 Hz/min, and the total measuring time is 399.6 s.

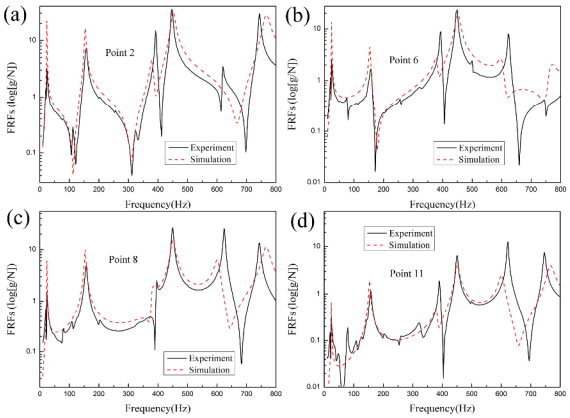

Fig. 19. Comparison of the FRFs on the rectangular plate without PDs between the simulation results and experimental data.

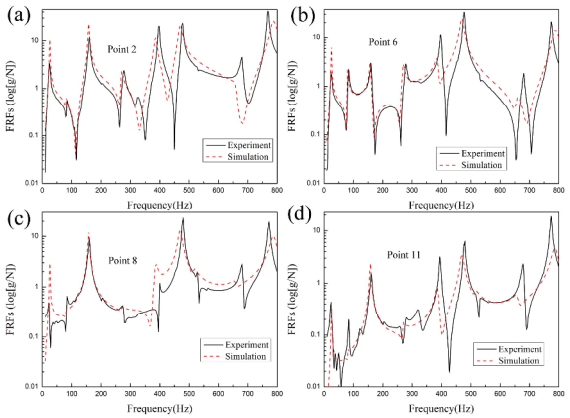

Fig. 20. Comparison of the FRFs on the rectangular plate with PDs between simulation results and experimental data.

The sampling rate is 8192 Hz. The FRFs are measured by an SO analyzer. The curve of the FRFs in each observation point is compared with the experiment results when the plates are with and without PDs (mass packing ratio is 50%). We also use the same four observation points for comparison and verification of the accuracy of the simulation results in Sec. 3. These points are 2, 6, 8 and 11 (Fig. 6).

Fig. 19 presents a comparison of the FRFs (acceleration/force) of the cantilever rectangular plate without PDs between the simulation results and experimental data. The simulation curves fit well with the measured curves from the experiment within the range of 0-800 Hz.

Remarkably, the simulation results in COMSOL differ slightly from the experimental results; structural damping considered in the simulation model is not exactly the actual intrinsic structural damping of the plate in the experiment. A similar trend is observed in Figs. 19 and 20 for harmonic excitation. The amplitude peak in the FRFs shifts in the simulation results compared with the case of the experimental data. In this case, such a phenomenon is possibly caused by the connection type between the rectangular plate and electromagnetic shaker (Fig. 18), which are connected by an adhesive. Obviously, the adhesive is an additional constraint condition for the boundary conditions of the rectangular plate, which leads to natural frequency shifts. This constraint is not exerted on the plates in the simulation.

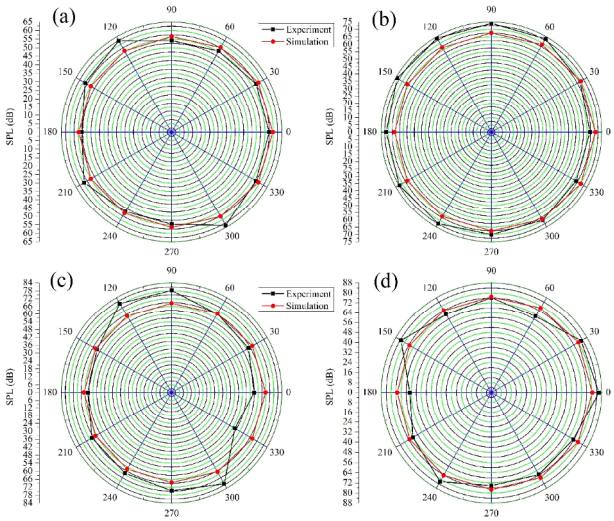

Fig. 21. Comparison of the far-field SPL of the plate without PDs at a radius of 1000 mm in the *x*-*y* plane between simulation results and experimental data.

Fig. 20 presents a comparison of the FRFs (acceleration/force) of the cantilever rectangular plate with PDs between the simulation results and experimental data. This figure shows that the acceleration responses between the theoretical results and experimental data agree well. Differences also exist at the amplitude peaks in the vicinity of the natural frequencies between the numerical and experimental responses for the plate with PDs. These differences stem from the hypothesis considered when modeling the system. Nevertheless, the simulation results show the ability of the model developed in this work to predict the dynamic behavior of the structure, considering the effect of particle damping for a wide frequency range. The results also prove that the theoretical model based on multiphase flow theory of gas particle is efficient for estimating the vibration response of the particle damping plate.

4.2 Acoustic radiation vibration

Another series of tests is conducted to identify the effect of PD on the acoustic radiation response of the system versus the excitation frequency. The polar plot of the far-field SPL at a radius of 1000 mm in the *x*-*y* plane is measured. A sine sweep excitation is used with 50, 150, 400 and 600 Hz.

Figs. 21 and 22 show the polar plot of the SPL of the simulation and experiment when the plate is without and with PDs, respectively. Good correlations are obtained between the analytical results and experimental data.

Differences also exist within a certain azimuth range be-

Table 4. Comparison of SPL mean value in the far-field at a radius of 1000 mm in the *x-y* plane for the plate without PDs.

Excitation frequency (Hz)	Mean value (dB)		Relative error
	Experiment	Simulation	
50	57.40	57.07	0.58%
150	70.90	68.19	3.83%
400	69.25	69.03	0.32%
600	77.03	77.72	0.89%

Table 5. Comparison of SPL mean value in the far-field at a radius of 1000 mm in the *x-y* plane for the plate with PD.

Excitation frequency (Hz)	Mean value (dB)		Relative error
	Experiment	Simulation	
50	54.72	53.72	1.8%
150	65.82	63.83	3%
400	63.87	64.06	0.29%
600	67.87	68.82	1.40%

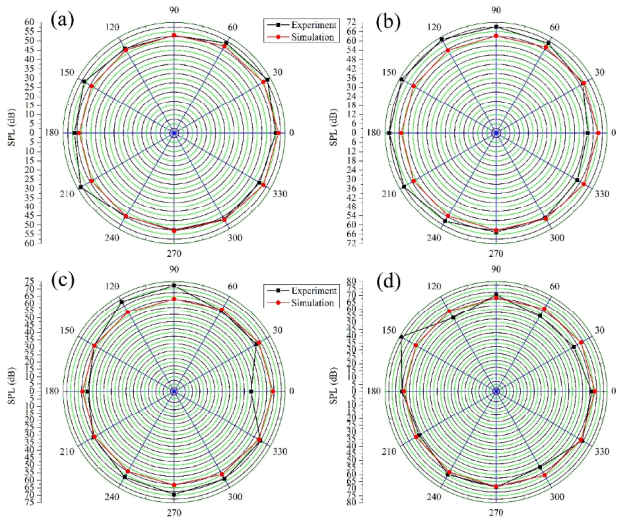

Fig. 22. Comparison of the far-field SPL of the plate with PDs at a radius of 1000 mm in the *x-y* plane between simulation results and experimental data.

tween the numerical and experimental results for the plate without and with PDs. Figs. 21(b) and 22(b) show that the SPL values of the experiment are larger than those of the simulation within the angle range of 30°-270°. However, the SPL values of the experiment are smaller than those of the simulation within the angle range of 0°-30° and 330°-360° in Figs. 21(c) and 22(c), respectively. On the contrary, the SPL values of the experiment are larger than those of the simulation within the angle range of 60°-150°.

For a better view of the comparison, the mean values (SPL) of the experiment in the far-field at a radius of 1000 mm in the *x-y* plane are compared with those of the simulation, as shown in Tables 4 and 5. Based on the simulation model, the simulation data are compared with the experimental data; the fractional error between the data is within 3.83% when the plate without PDs is excited at 50, 150, 400 and 600 Hz (Table 4).

Table 5 lists the predicted mean values (SPL). These values are compared with the measured overall mean values, with a maximum error of 3% when the plate with PDs is excited using the same excitation frequencies.

Notably, the two curves between simulation results and experimental data do not match perfectly in Figs. 21 and 22 because the value of the mesh used is coarse in the model. The size of the mesh in the model is set to the default setup of this model, which is not sufficiently fine. Finer mesh is suited to resolve the acoustic boundary layer. The coarse mesh is selected to reduce the required memory to about 4 GB of RAM.

These aforementioned errors possibly stem from the hypothesis considered when modeling the system. First, we ignore the interaction between particles and wall of enclosure, and we use numerical analysis methods to obtain the model expression of equivalent nonlinear viscous damping. The theoretical model is not a complete description for particle damping but only an approximate expression. Second, the exciter is attached to the plates in the experiment, which actually causes another constraint to the plates; nevertheless, this constraint is not exerted on the plates in the simulation. Third, every condition and material property is ideal in the simulation; however, the plates used in the experiment are not made of uniform aluminum alloy sheet. The actual values of Young's modulus, Poisson's ratio, and structural damping coefficient are difficult to obtain. Based on the abovementioned factors, the accuracy of simulation is affected. Nevertheless, the analysis of the simulation results of the structure with PDs shows the ability of the model developed in this work to predict the vibration and acoustic radiation response of the continuous structure, considering the effect of particle damping. Compared with the DEM simulation, this theoretical model is less time consuming and presents calculation ease and wider applicability.

The theoretical model based on multiphase flow theory of gas particle is efficient for estimating vibration and acoustic radiation of the particle damping structure with good accuracy and reliability.

5. Conclusion

To predict the vibration and acoustic radiation responses of particle damping composite structures rapidly and effectively, combined studies of theoretical derivation, numerical simulation, and experimental research are conducted. An analytical model based on two-phase flow theory of gas particle is developed, in which equivalent viscous damping for interparticle collisions and friction is introduced. The sound-structure interactions of the plate with PDs is solved using a self-developed analysis model combined with a COMSOL Mul-

tiphysics model. Investigating the performance of particle damping using this method is convenient, which makes the entire model convenient for further in-depth studies. An experimental verification process to evaluate the validity of the theoretical model is carried out to study the vibration and acoustic radiation characteristics of particle damping plates. The results of the simulation show excellent agreement with those obtained from the experiment. The following conclusions are drawn from this study. For particle damping plate, the PDs are effective to restrain the vibration of the structure and attenuate the far-field sound pressure of the host structures. As a sort of passive technology, PD shows high efficiency over a wide frequency range. PD as an added mass type of passive vibration device should make the inherent frequencies shift and decrease because of the added mass. The theoretical model based on multiphase flow theory of gas particle is efficient for estimating vibration and acoustic radiation of particle damping plate with good accuracy and reliability. Compared with DEM simulation, this theoretical model is less time consuming and presents calculation ease and wide applicability.

The prediction accuracy of the theoretical model developed in this paper should be improved, and further research and experiments should be conducted. The above questions will be studied further in subsequent work. The present work will help stimulate more developments in particle damping technology, specifically toward understanding the damping behavior characteristics to facilitate design.

In conclusion, the research results show that the analytical model based on two-phase flow theory of gas particle is simple and effective. This study does not only lay an important theoretical foundation for the further study of the vibration and acoustic radiation of the particle damping composite structure, but it also provides important theoretical guidance for low-noise optimization design of particle damping structures. Furthermore, the proposed model has an important reference value for the noise control of such structures.

Acknowledgement

The work described in this paper was supported by the Natural Science Foundation of China (No. 51075316).

Nomenclature

μ_c : Effective viscosity caused by interparticle collisions
e_p : Restitution coefficient of the particle
α_p : Packing ratio defined as the volume of particles to the total volume of the cavity
ρ_p : Density of particles
d_p : Diameter of particles
Θ : Fluctuation-specific kinetic energy
g_p : Radial distribution function
ϕ : Angle of internal friction
I_{2D} : Second invariant of the deviatoric stress tensor
p_p : Solid pressure
μ_m : Viscosity of the gas particle mixture flow
μ_g : Viscosity of gas
d : Diameter of the cavity
h : Height of the cavity
ρ_m : Equivalent volume density of the mixture flow related to the densities of the gas and particle
$|\dot{x}|$: Amplitude of vibration velocity
f : Excitation frequency
$\mathbf{X}$: Nodal displacement of the whole system
$\mathbf{F}$: External force applied to the system
$\mathbf{K}$: Stiffness of the plate with PDs
$\mathbf{M}$: Mass matrix of the plate with PDs
$\mathbf{p}$: Pressure to the solid wall
$\mathbf{n}_s$: Outward-pointing unit normal vector observed from inside the solid domain
p : Pressure (N/m^2)
$\mathbf{u}$: Calculated harmonic-displacement vector of the solid structure
$\mathbf{n}_a$: Outward-pointing unit normal vector observed from inside the acoustics domain
$\mathbf{q}$: Optional dipole source (m/s^2)
p_o : Amplitude of a harmonic pressure source
R_{pml} : Absorbing perfectly matched layer
p : Scattered field
α_{mp} : Mass packing ratio

References

[1] T. Chen et al., Dissipation mechanisms of non-obstructive particle damping using discrete element method, *Proceedings of SPIE International Symposium on Smart Structures and Materials,* Newport, California (2001).
[2] J. R. Fricke, Lodengraf damping: An advanced vibration damping technology, *Sound and Vibration,* 34 (7) (2000) 22-27.
[3] S. S. Simonian, Particle beam damper, *Society of Photo-Optical Instrumentation Engineers (SPIE) Conference Series,* San Diego, California (1995).
[4] R. D. Friend and V. K. Kinra, Measurement and analysis of particle impact damping, *1999 Symposium on Smart Structures and Materials,* Newport Beach, CA (1999).
[5] L. F. Bryce, M. F. Eric and E. O. Steven, Effectiveness and Predictability of Particle Damping, *SPIE's 7th Annual International Symposium on Smart Structures and Materials,* Newport Beach, CA (2000).
[6] N. Popplewell and S. E. Semercigil, Performance of the bean bag impact damper for a sinusoidal external force, *Journal of Sound and Vibration,* 133 (2) (1989) 193-223.
[7] A. L. Paget, Vibration in steam turbine buckets and damping by impacts, *Engineering,* 143 (1937) 305-307.
[8] L. J. Bain, *Impact damping of printing cylinders*, P.a.T. Office, Editor Google Patents: U.S. (1978).
[9] K. P. Duffy, G. V. Brown and R. L. Bagley, *Self-tuning impact damper for rotating blades*, P.a.T. Office, Editor

Google Patents: U.S. (2004).
[10] E. Prottengeier and H. Siegner, *Reversible impact damper, in particular for vehicles*, P.a.T. Office, Editor Google Patents: U.S. (1993).
[11] R. D. Rocke and S. F. Masri, Application of a single-unit impact damper to an antenna structure, *Shock Vib. Bull.* (39 Part 4) (1969) 1-10.
[12] M. M. Sadek, Impact dampers for controlling vibration in machine-tools, *Machinery and Production Engineering,* 120 (3090) (1972) 152-161.
[13] I. Masanobu et al., Effectiveness of the particle damper with granular materials, *3rd International Conference on Integrity, Reliability and Failure,* Porto, Portugal (2009).
[14] Y. Isao, T. Yoshito and N. Y. So, Particle damping with granular materials for multi-body system, *ICSV 15 Internation Congress on Sound and Vibration,* Daejeon, Korea (2008).
[15] R. D. Friend and V. K. Kinra, Particle impact damping, *Journal of Sound and Vibration,* 233 (1) (2000) 93-118.
[16] M. Trigui et al., An experimental study of a multi-particle impact damper, *Proceedings of the Institution of Mechanical Engineers, Part C: Journal of Mechanical Engineering Science,* 223 (9) (2009) 2029-2038.
[17] C. Salueña, T. Pöschel and S. E. Esipov, Dissipative properties of vibrated granular materials, *Physical Review E,* 59 (4) (1999) 4422-4425.
[18] K. Mao et al., Simulation and characterization of particle damping in transient vibrations, *Journal of Vibration and Acoustics,* 126 (2) (2004) 202-211.
[19] Z. Lu, X. Lu and S. F. Masri, Studies of the performance of particle dampers under dynamic loads, *Journal of Sound and Vibration,* 329 (26) (2010) 5415-5433.
[20] P. A. Cundall and O. D. L. Strack, A discrete numerical model for granular assemblies, *Geotechnique,* 29 (1) (1979) 47-65.
[21] V. P. Legeza, Dynamics of vibroprotective systems with roller dampers of low-frequency vibrations, *Strength of Materials,* 36 (2) (2004) 185-194.
[22] H. Zhou and Q. Chen, Verifications of the damping properties of particle dampers, *Proceedings of The Third Asian Conference on Multibody Dynamics,* Tokyo, Japan (2006).
[23] P. A. Cundall and O. D. L. Strack, The development of constitutive laws for soil using the distinct element method, *Numerical Methods in Geomechanics,* 1 (1979) 289-317.
[24] X.-M. Bai et al., Investigation of particle damping mechanism via particle dynamics simulations, *Granular Matter*, 11 (6) (2009) 417-429.
[25] L. F. Bryce, M. F. Eric and E. O. Steven, Design methodology for particle damping, *SPIE's 8th Annual International Symposium on Smart Structures and Materials,* Newport Beach, CA (2001).
[26] M. Saeki, Analytical study of multi-particle damping, *Journal of Sound and Vibration,* 281 (3) (2005) 1133-1144.
[27] C. X. Wong, M. C. Daniel and J. A. Rongong, Energy dissipation prediction of particle dampers, *Journal of Sound and Vibration,* 319 (1) (2009) 91-118.
[28] C. J. Wu, W. H. Liao and M. Y. Wang, Modeling of granular particle damping using multiphase flow theory of gas-particle, *Journal of Vibration and Acoustics,* 126 (2) (2004) 196-201.
[29] X. Fang and J. Tang, Granular damping in forced vibration: Qualitative and quantitative analyses, *Journal of Vibration and Acoustics,* 128 (4) (2006) 489-500.
[30] C. J. Wu, R. C. Yang and D. Q. Wang, An improved modeling of granular particle damping using multiphase flow theory of gas-particle, *20th International Congress on Sound & Vibration,* Bangkok, Thailand (2013).
[31] C. Wu, R. Yang and D. Wang, Prediction on vibration response of a cantilever particle-damping beam based on two-phase flow theory of gas-particle, *Chinese Journal of Mechanical Engineering,* 49 (10) (2013) 53-61.
[32] D. Q. Wang et al., Forced vibration of the particle-damping beam based on multiphase flow theory of gas-particle, *21th International Congress on Sound & Vibration,* Beijing, China (2014).
[33] D. Wang and C. Wu, Vibration response prediction of plate with particle dampers using cosimulation method, *Shock and Vibration,* 501 (2015) 270398.
[34] L. S. Fan and C. Zhu, *Principles of gas-solid flows*, Cambridge University Press, Cambridge (1998).
[35] D. G. Schaeffer, Instability in the evolution equations describing incompressible granular flow, *Journal of Differential Equations,* 66 (1) (1987) 19-50.
[36] C. K. K. Lun et al., Kinetic theories for granular flow: inelastic particles in Couette flow and slightly inelastic particles in a general flowfield, *Journal of Fluid Mechanics,* 140 (1) (1984) 223-256.
[37] R. D. Blevins, *Flow-induced vibration,* 2nd ed., Von Nostrand Reinhold, New York (1990).
[38] T. Sarpkaya, Force on a circular cylinder in viscous oscillatory flow at low Keulegan-Carpenter number, *J. Fluid. Mech.,* 165 (1986) 61-71.
[39] K. Mao et al., DEM simulation of particle damping, *Powder Technology,* 142 (2) (2004) 154-165.
[40] M. Trigui, E. Foltete and N. Bouhaddi, Prediction of the dynamic response of a plate treated by particle impact damper, *Proceedings of the Institution of Mechanical Engineers, Part C: Journal of Mechanical Engineering Science,* 228 (5) (2014) 799-814.
[41] Z. Xu, M. Y. Wang and T. Chen, Particle damping for passive vibration suppression: numerical modelling and experimental investigation, *Journal of Sound and Vibration,* 279 (3) (2005) 1097-1120.
[42] D. Wang and C. Wu, Parameter estimation and arrangement optimization of particle dampers on the cantilever rectangular plate, *Journal of Vibroengineering,* 17 (5) (2015) 2503-2520.
[43] P. Veeramuthuvel et al., Prediction of particle damping parameters using RBF neural network, *Procedia Materials Science,* 5 (2014) 335-344.

Dongqiang Wang was born in China in 1984. He is now a Doctoral candidate in the School of Mechanical Engineering of Xi'an Jiaotong University (XJTU). He has been with XJTU since September, 2012. His research fields include particle damping technique and vibration and noise control.

ChengJun Wu completed his Ph.D. on sound and structural interaction at XJTU in 1999. He is now a professor in the Institute of Vibration and Noise Control, School of Mechanical Engineering of XJTU. His research fields include structural-acoustic interaction, modal analysis and dynamic optimization design, acoustic prediction and CFD simulation, passive vibration and noise control, particle damping, and viscoelastic damping.